北見工業大学研究報告
第19巻 第1号 (昭和62年)

Memoirs of the Kitami Institute of Technology
Vol. 19 No. 1 (1987)

Evaluation of the First Order Kinetic Approximation in Heterogeneous Catalysis*

by Tohru KANNO**, Takuma KIMURA***, Takanobu ONOSE**
Masatoshi HAYASHI**** and Masayoshi KOBAYASHI**

(Received April 30, 1987)

Abstract

The validity of first order kinetic approximation in heterogeneous catalysis has been evaluated by using the transient response method. As an example of a solid catalysed reaction, the oxidation of carbon monoxide has been studied on four different metal oxides MnO_2, Cr_2O_3, Pb_3O_4, and ZnO. The steady state rate analysis apparently met first order kinetics with respect to the concentration of CO for all the catalysts. The Arrhenius plots of the apparent first order rate constant obtained clearly gave a good straight line and estimated the apparent activation energy of the reactions on each catalyst.

A simple first order kinetic model due to surface reaction controlling is proposed to explain the transient state and the steady state of reaction. Based on the models proposed, the transient response curves of carbon dioxide caused by the stepwise change in the concentration are simulated by using personal computers. The results exhibit a large deviation of the calculated curves from the experimental ones especially at the transient state whereas the steady state values of both are in good agreement.

Four different dual path models have separately been proposed for each of the four catalysts. The models consistently explain the characteristic mode of the transient response curves obtained for each catalyst and under wide experimental conditions. The activation energy of the slowest elementary step is evaluated for all the catalysts, and some of the values deviate largely from those estimated from the apparent first order kinetic models.

1. Introduction

As is well known, a large number of reactions in heterogeneous catalysis apparently obey first order kinetics depending on the experimental conditions. When one can get the first order kinetic data, one may usually arrive at the following similar conclusions :

(1) adsorption controlling,
(2) surface reaction controlling,
(3) a small amount of accumulation of reactants and products,
(4) no inhibition effect of the adsorption of products on the surface reaction rate.

* The paper was partly presented at the Hokkaido regional meeting of the Chemical Society of Japan in the winter period of 1987.

** Department of Industrial Chemistry.
*** Chemical Environmental Engineering.
**** Makkari village office.

These explanations sometimes lead to the reaction mechanism being misunderstood. In addition, the turnover frequency (Nt, molecules sec^{-1}) has frequently been evaluated from the apparent first order rate constant and used to compare the catalytic activity of catalysts, even though this apparent rate constant is very different from the true surface reaction rate constant. It is necessary to know the detailed kinetic structure for a strict comparison of the surface reaction efficiency. A deep and interesting characteristic reaction sequence is usually hidden behind the apparent first order kinetic data[1~3]. One may easily visualize the detailed structure of those complex reactions by using the transient response method[4~7] In the present study, our purpose is to apply this method for the solution of the problem.

Carbon monoxide oxidation progresses easily on metal oxides and its kinetics typically indicates a first order with respect to the concentration of CO. Furthermore, as has been studied previously, their surface oxygen is widely distributed in oxidation power and adsorption strength. From this variety in the nature of the surface oxygen species one can recognize that the actual reaction mechanism is complex. Another purpose of this study is the application of the classification[7] of the mode of transient response curves to distinguish the multi-path reaction net work.

2. Experimental Procedure

(1) Catalysts

The physical nature of the four catalysts used in this study were presented in Table 1.

MnO_2: Two kinds of manganese dioxide, electrolytic manganese dioxide (E-MnO_2) and natural manganese dioxide (N-MnO_2) from Indonesia, were simultaneously used to compare the reaction kinetics. The catalysts were dried at 110°C for E-MnO_2 and 180°C for N-MnO_2 in the O_2 (20%)-N_2 mixture prior to

Table 1. Summary of the reaction parameters

		BET surface area (m^2/g)	Temp. (°C)	W (g)	U (cm/min)	L (cm)	ε	ρ_c (g/cm^3)	$q_{O_2}\times10^5$ (mol/g)	$q_{CO_2}\times10^5$ (mol/g)
MnO_2	E-MnO_2	31	−26− 60	39.3 (60–80 mesh)	728	83	0.5	1.94	1.28	3.30
	N-MnO_2	74	140–150							
Cr_2O_3	α-Cr_2O_3	21	105–172	55.2 (24–32 mesh)	304	140	0.75	5.75	I =3.30 II =1.17	3.30
Pb_3O_4		0.4	225–250	50 (42–60 mesh)	850	106	0.58	2.40	6.20	0.30
ZnO		4.4	190–250	68.1–189.6 (20–40 mesh)	221	154–55.3	0.56	1.70	I =0.073 II =0.27	0.27

use. The crystallographic structures of E- and N-MnO_2 were respectively analysed to be amorphous an β-manganese dioxide. Both were confirmed to be *n*-type semiconductors by measuring the Hall coefficient[8,9].

Cr_2O_3: The starting material was chromium trioxide which was decomposed at 450°C for 5 hrs in an air flow. The X-ray diffraction analysis showed α-Cr_2O_3 of the sample. The electrical conductivity change of the sample clearly behaved as a typical p-type semiconductor for the adsorption of oxygen[10].

Pb_3O_4: The catalyst was prepared by the thermal decomposition of lead nitrate ($(Pb(NO_3)_2)$) which was supplied from Wako Pure Chemicals Co. The white powder was carefully decomposed into β-PbO (yellow) at 370-390°C in an air flow, because the sample was easily converted into α-PbO (red-brown) when the temperature became higher than 400°C. The yellow powder was slowly heated by using a temperature program controller at 10°C/min in air flow up to 470°C, and then the sample was treated by a pure oxygen flow at 470°C for 30 hrs. The sample could thus be completely converted into red lead (Pb_3O_4)[11].

ZnO: A reagent grade commercial zinc oxide was used as a catalyst, which was supplied by Kanto Reagent Co[12].

More detailed characterization of the four catalysts can be found in previous papers[8~12].

(2) Cases and Analysis

The reaction gases used in this study were basically supplied from commercial cylinders. The purities of the gases were CO (99.95%), O_2 (99.9%), He (99.995%) and CO_2 (98.5%). In the case of MnO_2, the reaction gas stream was carefully dried by passing it through a Molecular Sieve 5A trap which was cooled at −78°C by a dry-ice methanol bath. For the other three catalysts, the gases were used with no further purification.

Two or three gas-chromatographs which were attached to the thermal conductivity detector were simultaneously employed to follow the rapid transient response of the outlet stream as continuously as possible. A Molecular Sieve 5A column and a Porapak Q column were separately used to analyse O_2, CO, and CO_2.

(3) Procedures

An ordinary tubular flow reactor (Pyrex or quartz glass) was commonly used under atmospheric pressure for all the catalysts. The amount of the catalyst was chosen so as to satisfy the necessity of the differential reactor for the total conversion of CO to be less than 10% as can be seen in Table 1. The external and internal gas diffusion effects were carefully confirmed to be negligible by changing the flow rate and the catalyst particle sizes. The longitudinal gas mixing effect was also confirmed to be negligible, because the delay from the step function was less than 10 seconds, a period which was negligibly smaller than the actual response period of longer than 10 minutes.

Special attention was paid to the change in the temperature of the catalyst bed. To easily remove the heat generation caused by the exothermic reaction,

a quartz tube reactor was used and immersed into a fluidized sand bath. The temperature change observed was within ±1°C at most. Attension was also paid to the fluctuation of the gas flow rate at the stepwise change in gas composition, and the accuracy of the flow rate was finely controlled within ±2 ml/min at most.

(4) Computer Simulation

Three personal computers (NEC PC 8001mkII) were used simultanously to compensate for their slow computing time. A high speed arithmetic processing unit was attached to each computer to shorten the computing time to less than one twenty fifth of the normal time.

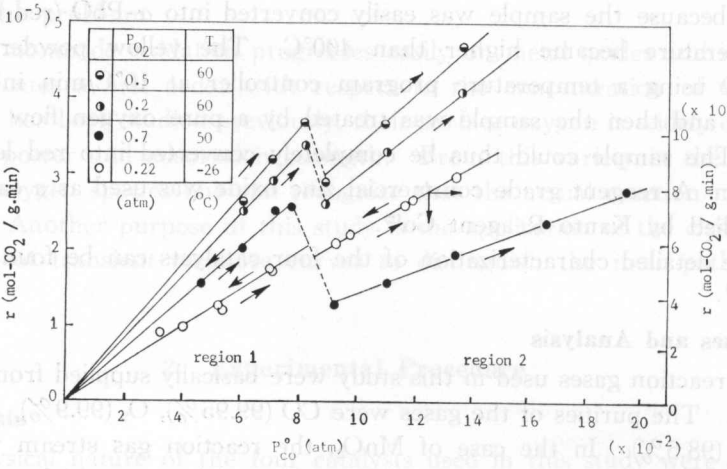

Fig. 1. Plots of r vs. P_{CO} for E-MnO_2

3. Experimental Results and Discussion

3-1. Presentation of the First Order Kinetic Model

MnO_2: Fig. 1 illustrates the first order dependency of the steady state rate on the concentration of CO in a wide range of temperature from −26 to 155°C using E- and N-MnO_2 (the results of N-MnO_2 are not presented), with no dependency on the kind of MnO_2 which was separately confirmed. One may recognize the anomalous change in the reactivity around $P_{CO}=0.07$ atm for all the temperature regions. The reason for this change has already been clarified in our previous papers as being the surface structure change from MnO_2 to Mn_2O_3. Our interest is that the rate has an apparent first order relation to P_{CO}. A large number of steady state rate data were gathered and carefully analysed by using more than ten kinetic models based on the Hougen-Watson procedure. Among these, three good models which were assumed to be surface rate controlling were chosen;

(1). *gaseous CO-dissociated oxygen atom* reaction model

$$r=\frac{K_O^{1/2}P_{O_2}^{1/2}}{1+K_O^{1/2}P_{O_2}^{1/2}}kP_{CO} \qquad (1)$$

(2). *gaseous CO-molecular oxygen* reaction model

$$r=\frac{K_{O_2}P_{O_2}}{1+K_{O_2}P_{O_2}}kP_{CO} \qquad (2)$$

(3). *adsorbed CO-dissociated oxygen atom* reaction model

$$r=\frac{K_{CO}K_{CO}^{1/2}P_{O_2}^{1/2}}{(1+K_O^{1/2}P_{O_2}^{1/2})^2}kP_{CO} \qquad (3)$$

where it is assumed that K_{CO} is negligibly small compared to K_O, and three equations can then be rearranged to linearize as follows, respectively;

$$P_{CO}/r=\frac{1}{K_O k}(P_{O_2}^{1/2})^{-1}+\frac{1}{k} \qquad (4)$$

$$P_{CO}/r=\frac{1}{K_{O_2}k}(P_{O_2})^{-1}+\frac{1}{k} \qquad (5)$$

$$(P_{CO}P_{O_2}/r)^{1/2}=\frac{K_O^{1/4}}{k^{1/2}k_{CO}^{1/2}}P_{O_2}^{1/2}+\frac{1}{k^{1/2}K_{CO}K_O^{1/4}} \qquad (6)$$

The experimental data showed commonly good straight lines based on these three equations (4), (5) and (6) as shown in Fig. 2. This agreement indicates that one can not distinguish the true reaction mechanism from the presented kinetic models.

Cr_2O_3: Fig. 3 illustrates the plots of rates vs. P_{CO}. The rate data roughly obey the first order expression on CO and zero order on O_2. The apparent first order rate constant(k_{ap}) is evaluated from the slope of the straight lines (broken

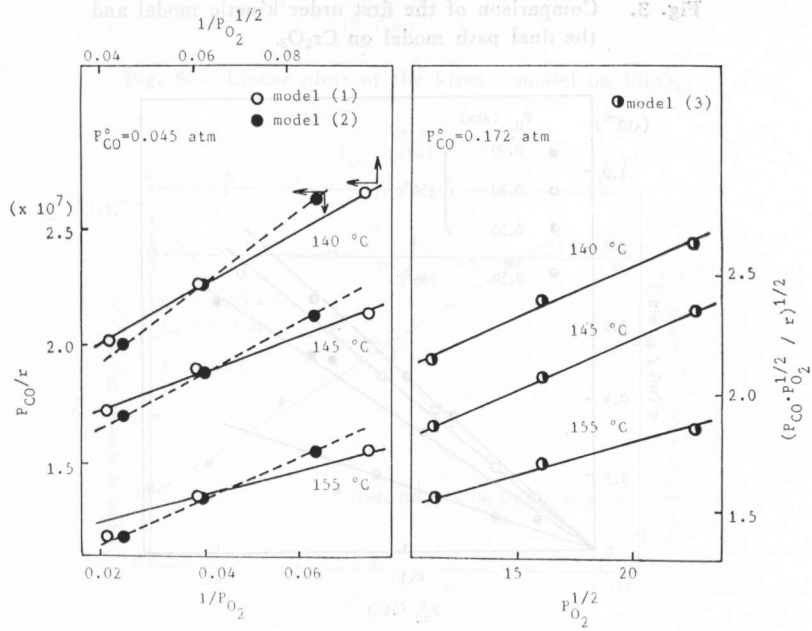

Fig. 2. Plots of the three kinetic models on N-MnO_2.

line), and the Arrhenius plots of k_{ap} obtained give a good straight line. The apparent activation energy is evaluated to be 130 kJ/mol. Since the amount of active sites is separately calculated to be 2.34×10^{-4} mol/g, the turnover frequency (N_t) may be evaluated as $0.064\sim1.6\times10^{-4}$ sec^{-1} depending on the reaction temperatures 105~172°C.

Pb_3O_4: The steady state rate clearly shows a good first order relation to

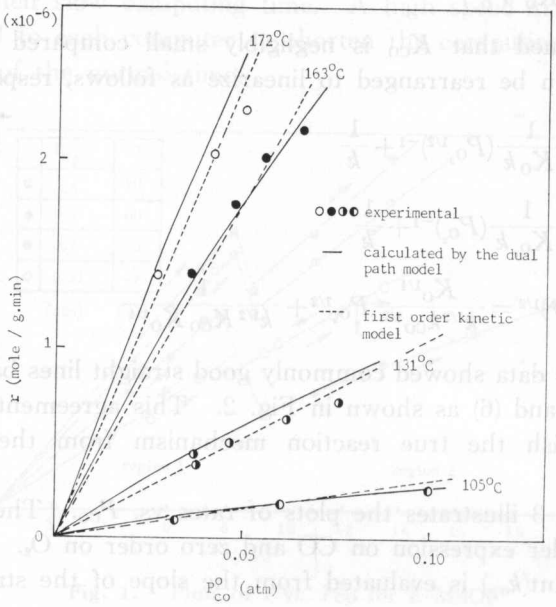

Fig. 3. Comparison of the first order kinetic model and the dual path model on Cr_2O_3.

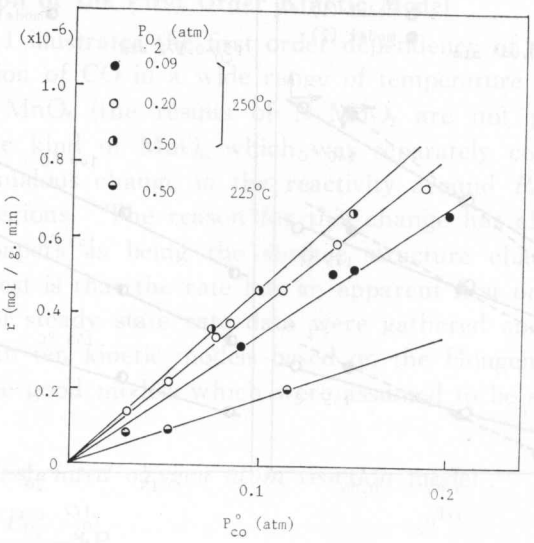

Fig. 4. Plots of r vs. P_{CO} on Pb_3O_4

P_{CO} as can be seen from Fig. 4. This first order relation is maintained at temperature in the range of 225~250°C and the concentration in the range of 9~50% O_2. The rate slightly increases with increasing concentration of O_2 as shown in Fig. 5 by a solid line. Equation (1) consistently explains all the rate data as can be seen from the broken line in Fig. 5. Fig. 6 illustrates that there is no effect of CO_2 on the reaction rate whereas an appreciable amount of CO_2 is adsorbed on the surface during the reaction. Here, the amount is evaluated from the graphical integrations of the transient response curves of CO_2. An adsorption isotherm obtained thus well fairly obeys the Langmuir equation as shown in Fig. 7. From the analysis of the isotherm, one may estimate the saturated amount of CO_2 adsorbed to be 3.0×10^{-6} mol/g. Assuming the satura-

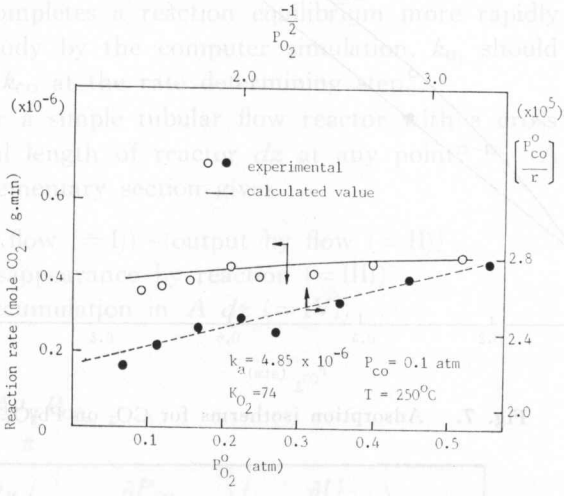

Fig. 5. Linear plots of the kinetic model on Pb_3O_4.

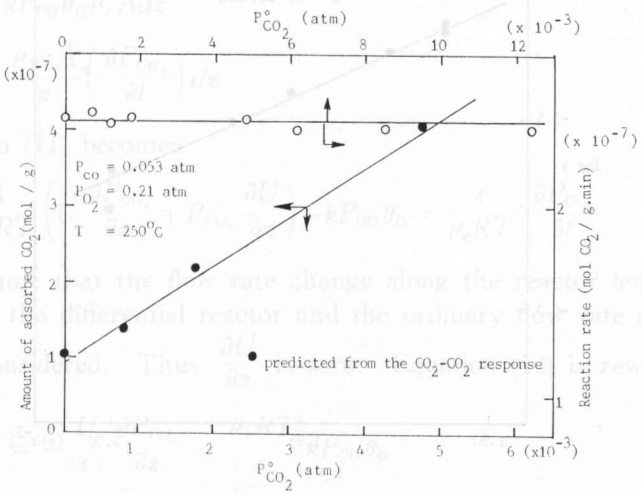

Fig. 6. The effect of CO_2 on r on Pb_3O_4.

tion of CO_2 adsorbed on the active site, the turnover frequency can be calculated to be $0.47 \sim 4.1 \times 10^{-3}\,sec^{-1}$ by using the rate of CO_2 formation in Fig. 4, depending on P_{CO} and temperature. The Arrhenius plots of k_{ap} give a good straight line as shown in Fig. 8 and estimates the activation energy to be 37 kJ/mol.

ZnO: The rate shows a simple first order relation to P_{CO} and zero order

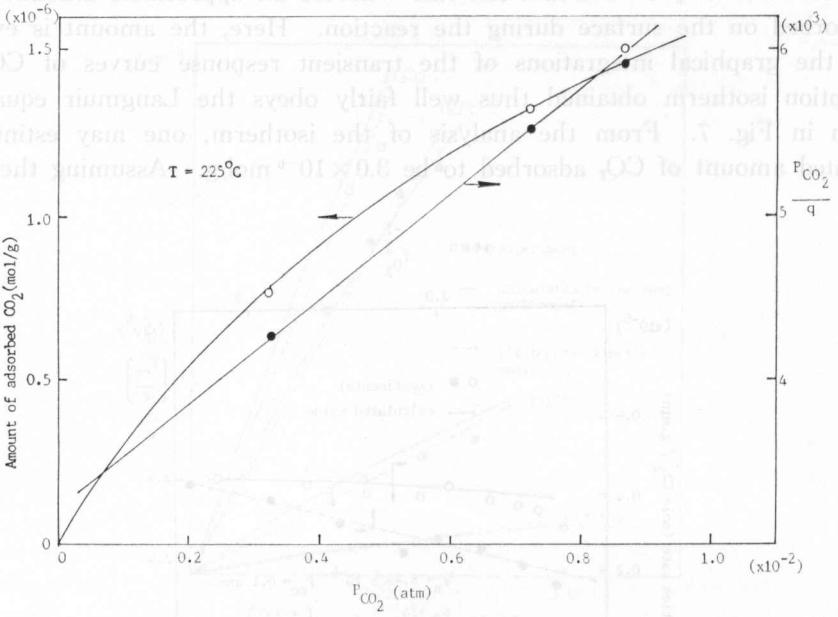

Fig. 7. Adsorption isotherms for CO_2 on Pb_3O_4.

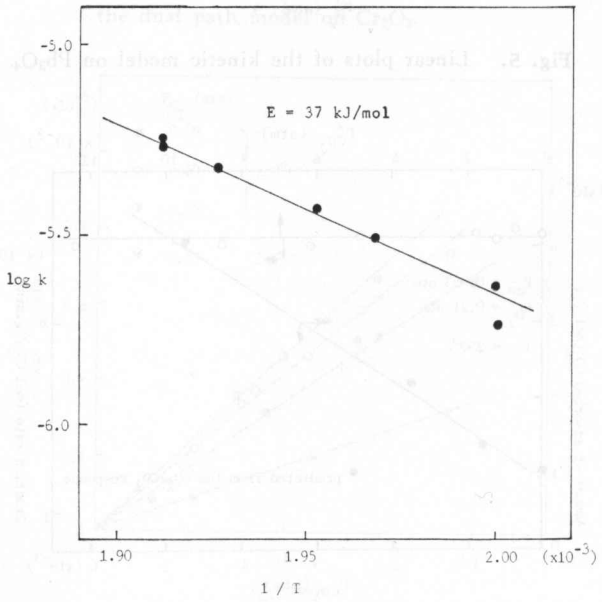

Fig. 8. Plots of $\log K$ vs. $1/T$ for Pb_3O_4.

to P_{O_2}. The activation energy is evaluated to be 104 kJ/mol from the Arrhenius plots of k_{ap}. The number of active sites is evaluated to be 3.43×10^{-6} mol/g, and then the turnover frequency can thus be calculated to be $0.24\sim7.3\times10^{-3}$ sec^{-1} using k_{ap} at $190\sim250$°C[12].

3-2. Computer Simulation of the Transient Response Curves Based on the First Order Kinetic Model

One can express the simple first order kinetic model as follows

$$CO\,(g)+O\cdot S \xrightarrow{k_{CO}} CO_2\,(g)+S \qquad (7)$$

$$O_2\,(g)+2S \xrightarrow{k_{O_2}} 2O\cdot S \qquad (8)$$

Where, step (8) completes a reaction equilibrium more rapidly than (7). Based on the detailed study by the computer simulation, k_{O_2} should be five hundred times larger than k_{CO} at the rate determining step.

First, consider a simple tubular flow reactor with a cross sectional area A and the differential length of reactor dz at any point[13~15]. A material balance of CO_2 for this elementary section gives

$$\begin{aligned}&(\text{input by flow } (=\text{I}))-(\text{output by flow } (=\text{II}))\\&\quad-(\text{disappearance by reaction } (=\text{III}))\\&\quad=(\text{accumulation in } A\ dz\ (=\text{IV}))\end{aligned} \qquad (9)$$

where

$$(\text{I})=\frac{UA\rho_M P_{CO_2}}{\pi} \qquad (10)$$

$$(\text{II})=\frac{A\rho_M}{\pi}\left(P_{CO_2}+\frac{\partial P_{CO_2}}{\partial z}dz\right)\left(U+\frac{\partial U}{\partial z}dz\right) \qquad (11)$$

$$(\text{III})=kP_{CO}\theta_O\rho_c A dz \qquad (12)$$

$$(\text{IV})=\frac{\rho_M\varepsilon A}{\pi}\left(\frac{\partial P_{CO_2}}{\partial t}\right)dz \qquad (13)$$

Hence, equation (11) becomes

$$-\frac{1}{\rho_M RT}\left(U\frac{\partial P_{CO_2}}{\partial z}+P_{CO_2}\frac{\partial U}{\partial z}\right)+kP_{CO}\theta_O=\frac{\varepsilon}{\rho_c RT}\frac{\partial P_{CO_2}}{\partial t} \qquad (14)$$

One may presume that the flow rate change along the reactor length should be negligible since the differential reactor and the ordinary flow rate at atmospheric pressure are considered. Thus $\dfrac{\partial U}{\partial z}$ is zero. Equation (14) is rewritten.

$$\frac{\partial P_{CO_2}}{\partial t}=-\frac{U}{\varepsilon}\frac{\partial P_{CO_2}}{\partial z}-\frac{\rho_c RT}{\varepsilon}kP_{CO}\theta_O \qquad (15)$$

Considering the differential reactor, the partial pressure of CO_2 might be

linearly distributed along the reactor length. One can thus estimate an arithmetic average of P_{CO_2} in the reactor. Equation (15) may be rearranged by the following ordinary differential equation

$$\frac{d}{dt}\frac{P^{\circ}_{CO_2}+P_{CO_2}}{2}=-\frac{U}{\varepsilon}\frac{P^{\circ}_{CO_2}-P_{CO_2}}{L}-\frac{\rho_c RT}{\varepsilon}k\frac{P^{\circ}_{CO}+P_{CO}}{2}\theta_O \tag{16}$$

where $P^{\circ}_{CO_2}=0$, $\dfrac{P^{\circ}_{CO}+P_{CO}}{2}\simeq P_{CO}$ and $\theta_O=\dfrac{P^{1/2}_{O_2}}{1+K^{1/2}_O P^{1/2}_{O_2}}(=1-\theta_V)$

Equation (16) becomes

$$\frac{dP_{CO_2}}{dt}=\frac{2U}{\varepsilon}P_{CO_2}-\frac{\rho_c RT}{\varepsilon}kP_{CO}\frac{1}{1+K^{1/2}_O P^{1/2}_{O_2}} \tag{17}$$

Equation (17) can easily be solved by using the following initial conditions

$$P_{CO_2}=P_{CO_2}{}^{i}$$
$$P_{CO}=P_{CO}{}^{i} \quad \text{at } t=0 \tag{18}$$

where the superscript i means initial steady state.

$$P_{CO}=(1-e^{-\alpha t})\,\beta P_{CO}+P_{CO_2}-\beta P_{CO}{}^{i} \tag{19}$$

Where $\alpha=\dfrac{2U}{\varepsilon L}$ and $\beta=\dfrac{L\rho_c RT}{U}k\theta_O$

at the reaction steady state, the following equation may be derived

$$\frac{U}{L\rho_c RT}P_{CO_2}=k\theta_O P_{CO}=r \tag{20}$$

Hence equation (20) corresponds to the reaction rate at the steady state.

Using equation (19), the transient response curves obtained on the four catalysts are simulated, and the typical results are shown in Figs. 9–16 by the broken lines. The calculated curves show a simple instantaneous response whereas the experimental ones indicate a characteristic mode with a delay depending on the catalysts. One may recognize a large deviation from the loci of the transient state whereas a good agreement is obtained at the steady state level. The first order kinetic approximation thereby cannot explain these specific modes at the initial stage of the response curves.

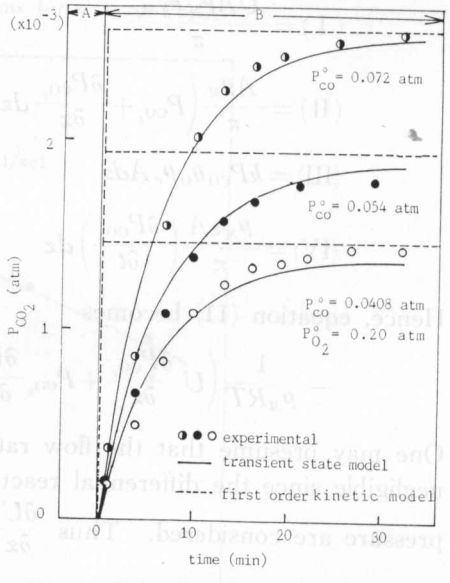

Fig. 9. CO–CO_2 responses on MnO_2. conditions A: $P^{\circ}_{He}=1.0$; B: ◑ $P^{\circ}_{CO}=0.072$, ● $P^{\circ}_{CO}=0.054$, ○ $P^{\circ}_{CO}=0.0408$ balanced by He.

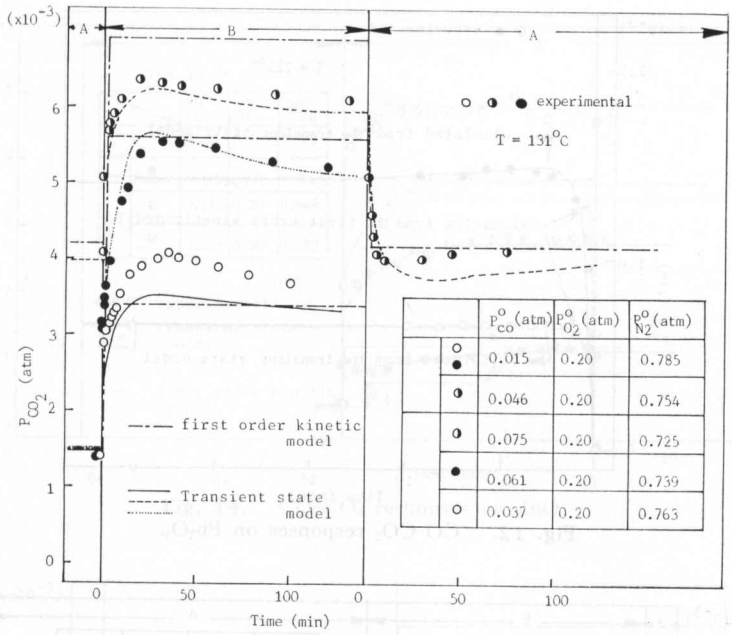

Fig. 10. CO–CO_2 responses on Cr_2O_3.

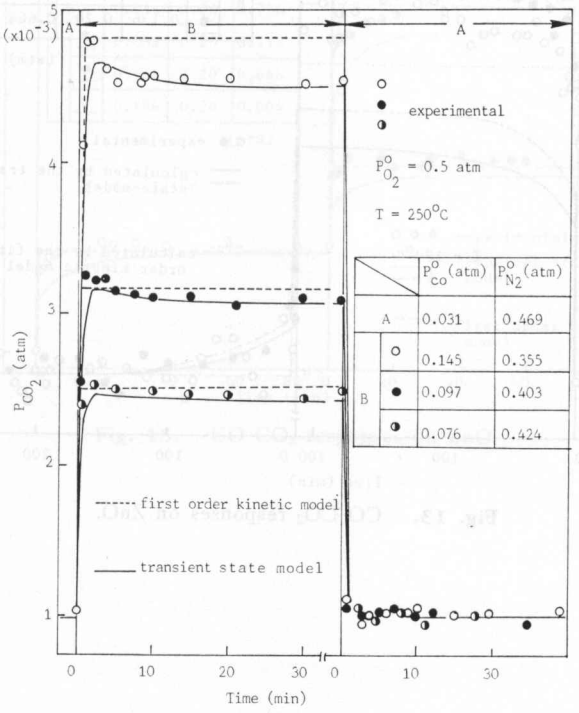

Fig. 11. CO–CO_2 responses on Pb_3O_4.

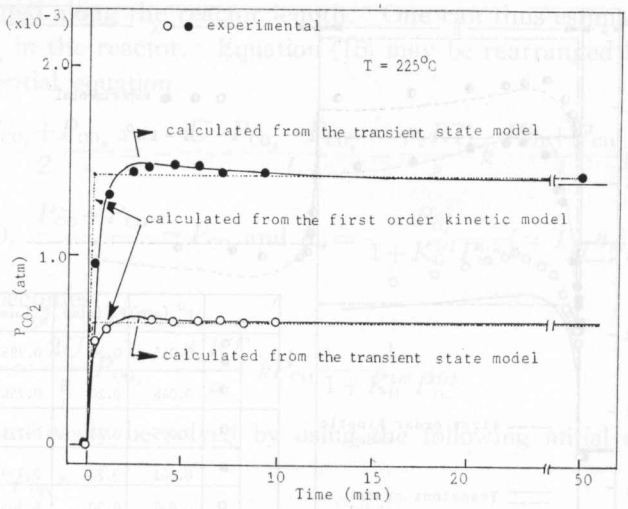

Fig. 12. CO–CO_2 responses on Pb_3O_4.

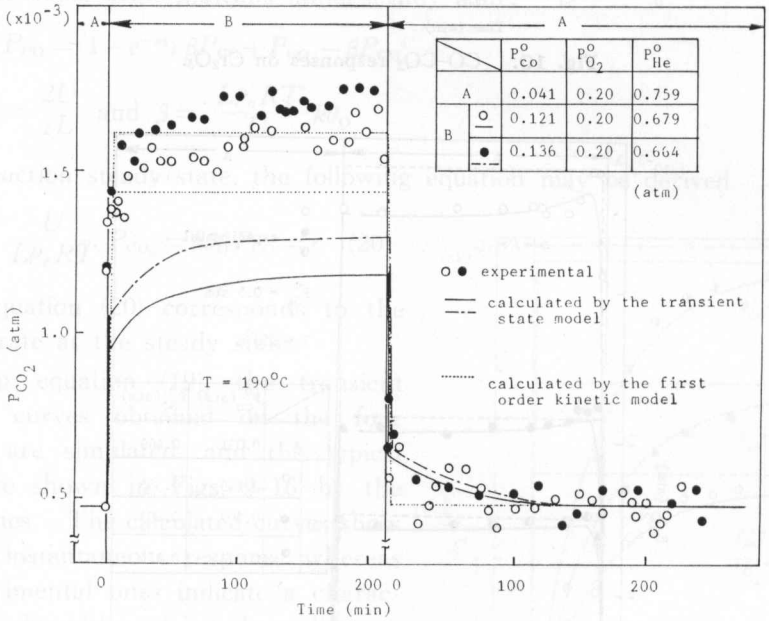

Fig. 13. CO–CO_2 responses on ZnO.

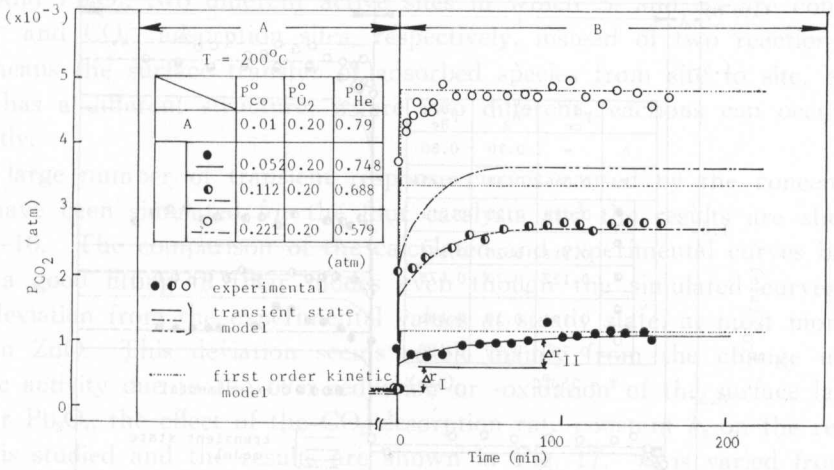

Fig. 14. CO–CO_2 responses on ZnO.

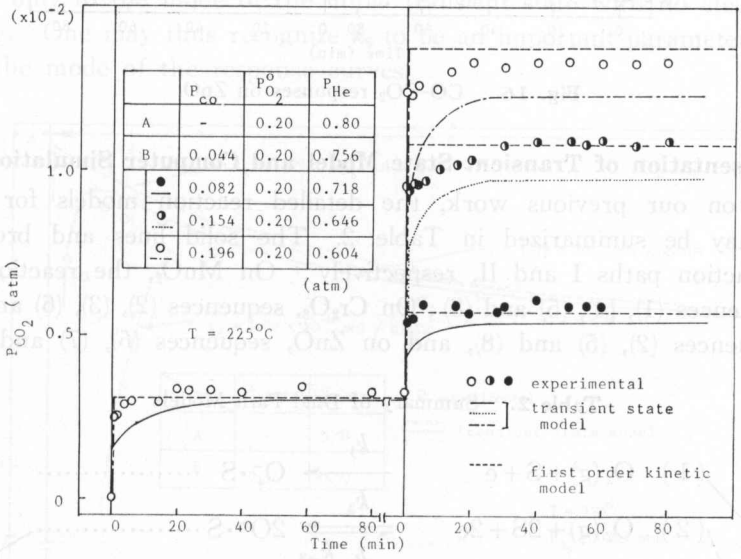

Fig. 15. CO–CO_2 responses on ZnO.

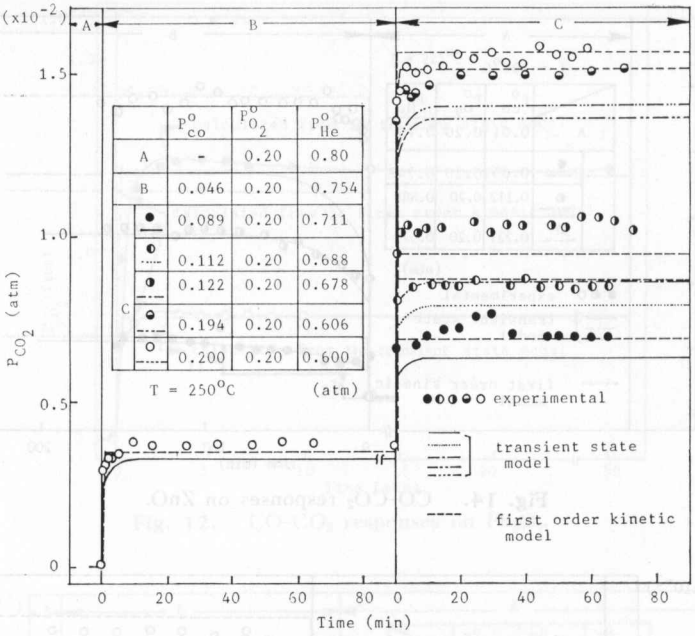

Fig. 16. CO–CO_2 responses on ZnO.

3-3. Presentation of Transient State Model and Computer Simulation

Based on our previous work, the detailed reaction models for the four catalysts may be summarized in Table 2. The solid lines and broken lines indicate reaction paths I and II, respectively: On MnO_2, the reaction consists of the sequences (1), (4), (5) and (8); On Cr_2O_3, sequences (2), (3), (6) and (8); On Pb_3O_4, sequences (2), (5) and (8), and on ZnO, sequences (6), (7) and (8). For

Table 2. Summary of Dual Path Models

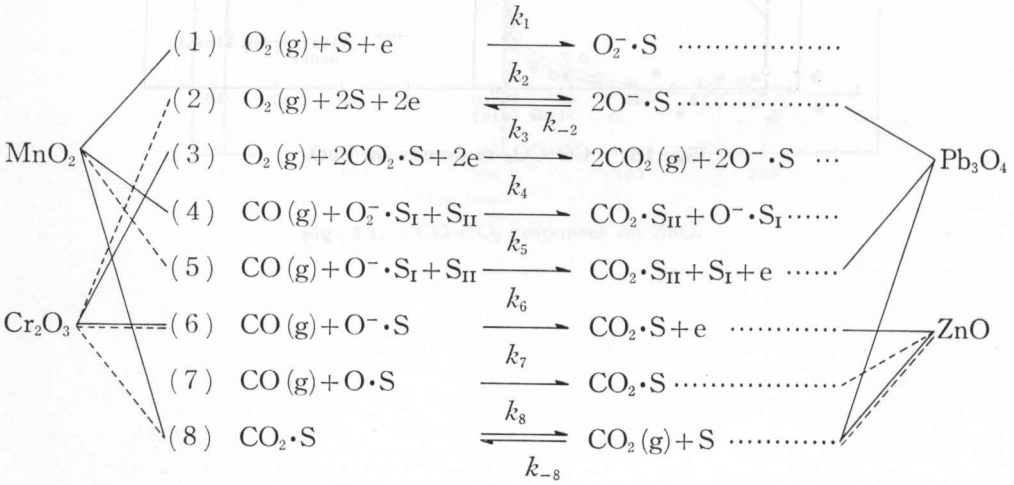

—— reaction path I, ····· reaction path II

MnO_2 and Pb_3O_4, two different active sites in which S_I and S_{II} are considered for O_2^- and CO_2^- adsorption sites, respectively, instead of two reaction paths. This means the surface transfer of adsorbed species from site to site, each of which has a different structure, where two different reactions can occur independently.

A large number of transient response curves caused by the concentration jump have been simulated for the four catalysts and the results are shown in Figs. 9-16. The comparison of the calculated and experimental curves basically shows a good fitting of their modes even though the simulated curves show a big deviation from the experimental values at steady state, at most more than 20% on ZnO. This deviation seems result mainly from the change in the catalytic activity due to the over-reduction or -oxidation of the surface layer.

For Pb_3O_4, the effect of the CO_2 desorption rate constant k_8 on the response curves is studied and the results are shown in Fig. 17. k_8 is varied from 10^{-6} to 10^{-4}, and the simulated curves tend to a steep overshoot mode with increasing magnitude of k_8, whereas the steady state value shows no change. Thereby, k_8 contributes only to the mode of the initial transient state with no change in the steady state. One may thus recognize k_8 to be an important parameter for characterizing the mode of the response curves.

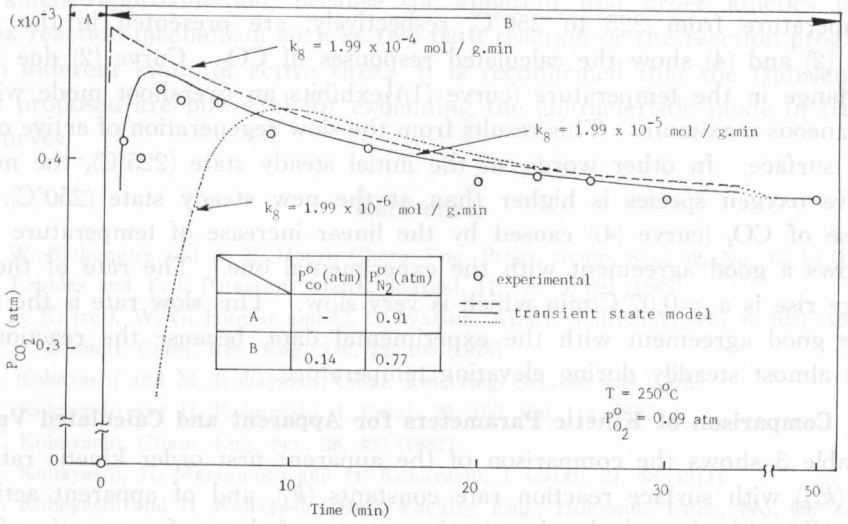

Fig. 17. The effect of k_8 on the response modes for Pb_3O_4.

The values of k_5 for Pb_3O_4 are evaluated in the temperature range from 225 to 250°C and the Arrhenius plots give the following equation

$$k_5 = 1.8 \times 10^{-3} \exp((-86200/R(T_0 + at))) \quad (21)$$

Using equation (21), the transient response of CO_2 caused by the stepwise or linear change in the temperature can easily be simulated, and the results are shown in Fig. 18. Temperature profiles for the stepwise and the linear increase

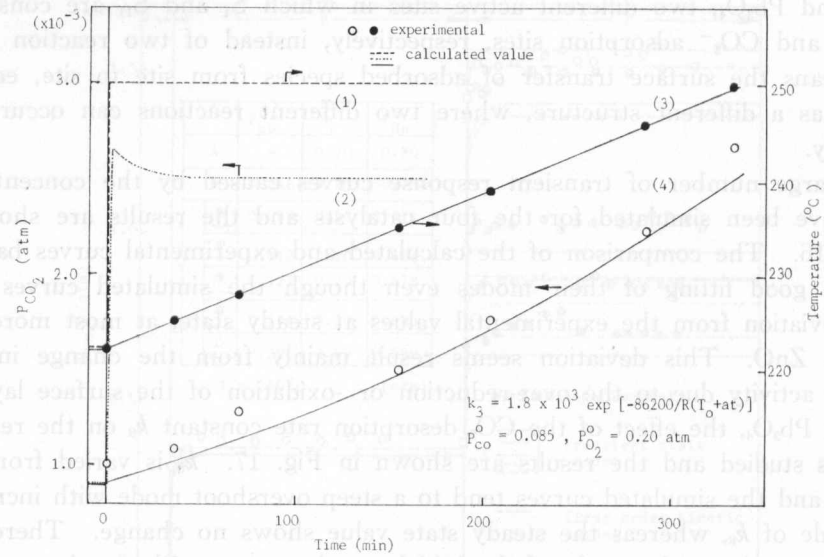

Fig. 18. Temperature -CO_2 responses on Pb_3O_4.
Curve (2) resulted from the temperature jump due to curve (1); curve (4) resulted from the linear temperature increase due to curve (3).

of temperature from 225 to 250°C, respectively, are presented in the figure. Curves (2) and (4) show the calculated responses of CO_2. Curve (2) due to the step change in the temperature (curve (1)) exhibits an overshoot mode with an instantaneous maximum. This results from the slow regeneration of active oxygen on the surface. In other words, at the initial steady state (225°C), the number of active oxygen species is higher than at the new steady state (250°C). The response of CO_2 (curve (4)) caused by the linear increase of temperature (curve (3)) shows a good agreement with the experimental one. The rate of the temperature rise is a =0.07°C/min which is very slow. This slow rate is the reason for the good agreement with the experimental data, because the reaction progresses almost steadily during elevating temperature.

3-4. Comparison of Kinetic Parameters for Apparent and Calculated Values

Table 3 shows the comparison of the apparent first order kinetic rate constants (k_{ap}) with surface reaction rate constants (k_j), and of apparent activation energy (E_a) with the calculated activation energy of the surface reaction for the four catalysts.

On Pb_3O_4, Cr_2O_3 (path II) and ZnO (Path I), the values of k_{ap} and k_j which is the slowest step are found to be close; $k_{ap}/k_5=0.98$, $k_{ap}/k_6=0.92$ and $k_{ap}/k_6=1.07$, respectively. For E-MnO_2 (path I), Cr_2O_3 (path I) and ZnO (path II), k_{ap} differs from k_j of the rate determining step indicating the populations $0.7\sim2.7$. This result indicates that one must pay special attention to evaluating the rate constant at the rate determining step from the apparent rate constant.

For a comparison between the apparent activation energy and the activation

Table 3. Summary of the Kinetic Parameters

	E_a (kJ/mol)	T (°C)	k_{ap} (mol/g·min·atm)	k_j (rate determining step) (mol/g·min·atm)	E_j (kJ/mol)	k_{ap}/k_j		E_a/E_j	
E-MnO_2	33	−26	7.0×10^{-5}	k_4(path I) 4.0×10^{-6} k_5(path II) 2.0×10^{-4}	—	path I 1.74	path II 0.035		
Cr_2O_3	130	131	1.1×10^{-5}	k_6 path I 4.15×10^{-6} path II 1.2×10^{-5}	path I E_6=396	path I 2.65	path II 0.92	0.33	
Pb_3O_4	37	250	4.9×10^{-6}	k_5 5.0×10^{-6}	E_5=26	0.98		1.42	
ZnO	104	190	2.8×10^{-7}	k_6(path I) 2.0×10^{-7} k_7(path II) 3.9×10^{-7}	path I E_6=107	path II E_7=15	path I 1.07	path II 0.72	path I 0.97	path II 6.93

k_j is presented in Table 2.

energy of the rate determining step, the ratio E_a/E_j is diversed 0.3∼7 suggesting the difficulty of the evaluation of E_j from E_a.

4. Conclusions

Some warnings have been proposed concerning the easy application of first order kinetic approximation, because the apparent first order kinetics hides a complex reaction mechanism such as two path reaction or the reaction progressing on two different kinds of active sites. It is reconfirmed that the transient state models proposed are powerful for explaining the characteristic mode of transient state curves.

References

1) J. W. Blakemore and A. E. Hoerl, Chem. Eng. Progr. Symp. Ser., **59**, No. 42, 14 (1963).
2) L. Lapidas and T. I. Peterson, AIchE. Journal, **11**, No. 5, 891 (1965).
3) J. R. Kittrell, W. G. Hunter and C. C. Watson, AIchE. Journal **11**, No. 6, 1051 (1965).
4) C. O. Bennett, Catal. Rev. Eng. Sci., **12**, 105 (1976).
5) H. Kobayashi and M. Kobayashi, Catal. Rev. Eng. Sci., **10**, 139 (1975).
6) M. Kobayashi and H. Kobayashi, J. Catal., **27**, 100, 108, 114 (1972).
7) M. Kobayashi, Chem. Eng. Sci., **39**, 393 (1982)
8) M. Kobayashi, H. Matsumoto and H. Kobayashi, J. Catal., **21**, 48 (1971).
9) M. Kobayashi and H. Kobayashi, Bull. Faculty Eng., Hokkaido Univ., **No. 69**, 221, 228 (1973).
10) M. Kobayashi and H. Kobayashi, Bull. Chem. Soc. Japan, **49**, 3009, 3018 (1976).
11) M. Kobayashi and H. Kobayashi, J. Catal. **36**, 74 (1975).
12) T. Kimura, T. Kanno, M. Hayashi and Kobayashi, Memoirs of the Kitami Inst. Tech., in print.
13) C. G. Lehr, S. Yurchak and R. L. Kabel, AIchE. Journal, **16**, No. 4, 627 (1968).
14) G. H. Denis and R. L. Kabel, AIchE. Journal, **16**, No. 6, 972 (1970).
15) G. H. Denis and R. L. Kabel, Chem. Eng. Sci., **25**, 1057 (1970).

Nomenclatures

A: cross sectional area of tubular reactor (cm^2)
a: rate of temperature rise (°C/min)
E_j: activation energy of the elementary step j (kJ/mol)
E_a: apparent activation energy (kJ/mol)
k_j: forward rate constant for step j (arbitrary unit, see Table 2)
k_{-j}: backward rate constant for step j (arbitrary unit, see Table 2)
K_j: equilibrium constant for step j (arbitrary unit)
L: total length of the catalyst bed (cm)
P_i°: partial pressure of i component at the inlet of the catalyst bed (atm)
P_i: partial pressure of i component at the outlet of the catalyst bed (atm)
q_m: saturated amount of adsorbed species i on the catalyst surface (mol/g)
R: gas constant (cm^3 atm K^{-1} mol^{-1})
S: active site
t: time elapsed after the step change of gas composition or the temperature change (min)
T: temperature (°K)
T_0: starting temperature for the temperature transient responses (°K)
U: superficial gas velocity (cm/min)
z: distance from the entrance of reactor (cm)

Greek symbols

ε: void fraction of packed bed reactor (—)
θ_i: surface coverage for adsorbed species i (—)
τ: total pressure (atm)
ρ_c: catalyst bed density (g/cm^3)
ρ_M: molar density (mol/cm^3)